Angle-resolved, mass-selected ion spectroscopy of carbon K-shell excited CF_3CCH

K. Okada [a], S. Tanimoto [a], T. Ibuki [b,*], Y. Haga [b], T. Gejo [c], K. Saito [a], K. Ohno [a]

[a] *Department of Chemistry, Hiroshima University, Higashi-Hiroshima 739-8526, Japan*

[b] *Kyoto University of Education, Fushimi-ku, Kyoto 612-8522, Japan*

[c] *Institute for Molecular Science, Okazaki 444-8585, Japan*

Received: 30 October 2003;

Abstract

Total photoabsorption cross section and peak assignments were presented for CF_3CCH in the carbon K-shell region. Anisotropy parameters of fragment ions obtained by means of an angle-resolved mass spectrometer were helpful to the peak assignments of the K-shell excitation into π* and σ* states. Kinetic energy distributions of the H^+, CH^+, C_2H^+ and CF_2^+ fragment ions were fitted using a Gaussian function with one peak, while those of the CF_3^+ fragment ion were analyzed by use of two and three components for the C K-shell excitation of the CF_3 and C_2H sides, respectively. The kinetic energy distribution of the CF_3^+ fragment ion was reasonably understood by the consideration that photofragmentation of the K-shell excited molecule probably competes with intramolecular energy relaxation in which the CF_3 group works as an effective energy reservoir. The yields of the CF_n^+ (n = 2,3), C_3FH^{2+} and $C_3F_2H^{2+}$ ions were dependent on the site of excitation.

* Corresponding author. Tel: +81-75-644-8276; Fax: +81-75-645-1734.
E-mail: ibuki@kyokyo-u.ac.jp (T. Ibuki).

1. Introduction

Angle-resolved ion spectroscopy has progressed for the last two decades in studying reaction dynamics of K-shell excited diatomic molecules randomly oriented in space [1–9]. One of the most meaningful results of the reaction dynamics is that the angular distribution $d\sigma/d\Omega$ of fragment ions produced after excitation with linearly polarized photons is expressed by the following equation within the axial recoil approximation [10–12]:

$$d\sigma/d\Omega = (\sigma_t/4\pi)[1 + \beta P_2(\cos\theta)], \quad (1)$$

where θ is the angle between the linearly polarized electric vector of the incident photons and the emitted photoion direction, β is the anisotropy parameter, and the Legendre polynomial $P_2(\cos\theta) = (3\cos^2\theta - 1)/2$. In the $\Delta\Lambda = \pm1$ transition such as the $\pi^* \leftarrow$ 1s excitation, the fragment ions are ejected in the direction perpendicular (90°) to the electric vector of the incident photon beam. In this case the anisotropy parameter $\beta = -1$ for a pure Π–Σ transition. The fragment ions formed via $\Delta\Lambda = 0$ transition such as $\sigma^* \leftarrow$ 1s are detected in a parallel direction (0°) and then $\beta = 2$ for a pure Σ_g–Σ_u transition. Since the middle of 1990s the usefulness of the concept in Eq. (1) has been applied in assigning the photoabsorption peaks and elucidating breakdown pathways of K-shell excited triatomic molecules [9,13–18].

The situation in a polyatomic molecule gets more complex: Photoabsorption peak of an electronically excited state is broaden because of the short lifetime, and a number of electronically excited states lie closely. It is essential to identify the fragment ions produced from a core-excited polyatomic molecule in order to study the reaction dynamics. In our previous works on the N and C

K-shell excited CF_3CN [19,20], the CF_3^+, CF_2^+, and CN^+ fragment ions with kinetic energies formed through the π^* state were ejected in a direction perpendicular to the linearly polarized electric vector of synchrotron radiation, and we argued that the bond dissociation after Auger electron emission competes with the intramolecular energy relaxation [20].

In this paper, we present the total photoabsorption cross section of CF_3CCH in the C K-shell region and propose the tentative peak assignments for the first time, giving the excitation energy of resonant state. For mass analysis at the resonant excitation energy we operated a time-of-flight mass spectrometer with two different modes: One of them is a linear time-of-flight (L-TOF) mass spectrometer and the other is a reflectron type time-of-flight (R-TOF) mass spectrometer. The ground state of CF_3CCH is a pseudo-linear molecule with the C–C≡C skeleton. Thus we applied the Eq. (1) to photofragmentation at the selected resonant states by using an angle-resolved L-TOF mass spectrometer. The L-TOF mode gives information about the anisotropy parameter and the kinetic energy distribution of the fragment ions. With the β values deduced and the kinetic energy distributions we discuss the dissociation dynamics of the C K-shell excited CF_3CCH. The site-specific photofragmentation of the C K-shell excited CF_3CCH was studied by using the R-TOF mass spectrometer.

2. Experimental

The experiments were performed on the soft X-ray beamline at the synchrotron radiation (SR) facility of the Institute for Molecular Science (IMS). The SR was monochromatized by a constant

deviation grazing incidence monochromator [21]. An Al thin filter was inserted downstream in order to suppress stray light. The energy resolution was typically $E/\Delta E$ = 2000–4000 in measuring total photoabsorption cross section. An energy resolution of about 1 eV was employed for acquisition of TOF mass spectra because of the weak photon flux of SR. The dispersed soft X-ray flux was monitored by a silicon photodiode and recorded simultaneously as a photocurrent in order to correct for fluctuations in the beam intensity. The photon energy was calibrated using the π^* transition of CO at 287.40 eV [22].

The TOF tube was mounted on the main chamber, which was rotatable from −20° to +110° angles with respect to the linearly polarized electric vector of SR. The L-TOF mass spectrometer was operated under Wiley–McLaren space focusing conditions [23]. The R-TOF mass spectrometer was designed to collect the fragment ions with kinetic energies up to ≈10 eV at m/e = 70. Mass discrimination effects in the R-TOF mode were minimized by applying high electrostatic fields of ±1.5 kV/cm for extracting fragment ions, by focusing the ions with two lens systems, and by measuring signal rates as low as possible. The experimental details were described in the previous paper [24]. The base pressure of the chamber was lower than 2×10^{-6} Pa and the sample was introduced into the chamber as an effusive jet.

The total photoabsorption cross section was acquired by using a Samson type double-ion chamber [25] with an Al thin filter at the front and the silicon photodiode at the end. The length of a plate to collect photoions was 10.0 cm. Sample pressure was measured using an MKS Baratron manometer and Lambert–Beer law was assumed. The sample was purchased from PCR Co. Ltd., and used without

further purification.

3. Results and discussion

3.1. Total photoabsorption cross section

The total photoabsorption cross section of CF_3CCH in the carbon K-shell region is shown in the top panel of Fig. 1. The experimental uncertainty for the photoabsorption cross section is estimated to be better than 10% of the given value judging from the stated accuracies of electrometers used and a pressure control system of the sample. The distinct peak at 285.1 eV is assigned to the $\pi^* \leftarrow$ C1s(CCH) resonant transition, where the K-shell electron is indistinguishable between the central C and the terminal CH of CF_3CCH. In the energy region higher than 287 eV some peaks are overlapped or embedded. We carried out a least-squares peak fitting by use of Gaussian functions in order to estimate the peak positions, and the results are shown in Fig. 1. The thin solid curves are the electronically excited states and the thick one is the sum of them. In the peak fitting we assumed that the lifetimes of the electronically excited states in the 287–298 eV region are close to that of the π^* resonant state at 285.1 eV.

The ionization potentials (IPs) for C 1s of the CF_3 and CCH groups have been reported to be 299.70 and 292.24 eV, respectively [26]. We think the latter IP of 292.24 eV is the mean value for the two K-shells in CCH. In $CF_3CH{=}CH_2$ and $CH_3C{\equiv}CH$ the IP of the central C 1s electron is 0.5 eV higher than that of C 1s in the terminal CH_2 or CH [26], and thus we estimate that the IPs of the K-shell electrons for the central C atom and the terminal CH group of CF_3CCH are 292.5 and 292.0 eV,

respectively. The peak positions deduced by the peak fitting, the term values, and the quantum defects are given in Table 1. We propose the tentative peak assignments: The peaks with $\delta = 1.2 \pm 0.1$ for the CCH group are assigned to the *n*s (*n* = 3, 4) Rydberg transitions and those with $\delta = 0.6 \pm 0.3$ are the *n*p (*n* = 3, 4) Rydberg levels. The peaks at 288.9 and 289.2 eV with the term values 3.1 and 3.3 eV, respectively, are assigned to the σ^*_{CH} and σ^*_{CC} transitions. The "de" means double excitation. The peaks in the 293–300 eV region are overlapped. The spectral shape, the peak positions, the term values and the quantum defects closely resemble those assigned to the C 1s excitation of CF_3 in CF_3CN [20]. Thus, the peak assignments for the C K-shell of CF_3 in CF_3CCH are given as shown in Table 1. The peaks at 294.0 and 295.4 eV are assigned to the π^* and σ^*_{CF} transitions, respectively, by taking account of the β values whose details are discussed in the following section. These assignments given above are consistent with those for CF_3CN [20] and CH_3CN [27].

3.2. Angle-resolved mass spectra

Figure 2 shows parts of L-TOF mass spectra observed in the $\sigma^*_{CF} \leftarrow$ C1s(CF) and $\pi^*_{C\equiv C} \leftarrow$ C1s(CCH) transitions at $h\nu$ = 295.4 and 285.1 eV, respectively. Panels (a) and (c) are the mass spectra detected in a direction perpendicular (90°) to the linearly polarized electric vector of SR, and the spectra in panels (b) and (d) are collected in the parallel (0°) direction. The contribution of background originating in the ionization of valence electrons was subtracted by measuring the L-TOF mass spectra at 282 eV. The profiles of the strongest CF^+ ion show little difference between the perpendicular and parallel directions. Thus the anisotropy parameter for CF^+ is $\beta \cong 0$ in Eq. (1), being ejected in an

isotropic direction. The spectral features of CF_3^+ and C_2H^+ detected in the perpendicular direction at $h\nu$ = 285.1 eV (Fig. 2c) have two 'wings' when they are compared with those in the parallel direction accompanying gently sloping shoulders (Fig. 2d). The wing in the low-mass region originates from the ions with kinetic energies initially moving toward the ion detector. The wing in the high-mass region comes from energetic ions initially moving away from the ion detector and then repelled back toward the ion detector by the applied electrostatic potential. The central part is produced by ions with zero or small kinetic energies. The energetic ions initially moving in a direction parallel to the electric vector of SR cannot reach to the ion detector located in the perpendicular position and vice versa.

The peak shape of fragment ion can be reproduced by fitting to a sum of components representing an assumed kinetic energy (KE) and angular distribution [28]. Kinetic energies of fragment ions and the anisotropy parameters in Eq. (1) for the components were determined so as to minimize the difference between the experimental data and the calculated profile. The linear polarization of SR was assumed to be 100% since the experimental degree of polarization was better than 98% [29]. The anisotropy parameters for the CF_3^+ fragment ion in Fig. 2 at the $\pi^* \leftarrow$ C1s(CCH) transition were deduced to be β = –0.49 for KE = 0.01, 0.048 and 0.12 eV; β = –0.52 for KE = 0.21, 0.34 and 0.49 eV; and β = –1 for KE = 0.67, 0.88, 1.12, 1.39, 1.69 and 2.02 eV. These combinations of β and KE were used to get an adequate fit. The β value and KE combinations for the C_2H^+ fragment ion were β = –0.20 for KE = 0.01, 0.06, 0.16, 0.30 and 0.49 eV; β = –0.35 for KE = 0.72, 1.0 and 1.32 eV; and β = –0.72 for KE = 1.69, 2.10, 2.56, 3.06, 3.61, 4.20 and 4.84 eV. The largest absolute values of β thus obtained are plotted in the lower panels of Fig. 1. The anisotropy parameters for the energetic CF_3^+,

CF_2^+, CF^+, C_2H^+ and CH^+ fragment ions were β = −1.0, −0.4, ≅0, −0.72, and −0.91 in the $\pi^* \leftarrow$ C1s(CCH) transition at 285.1 eV, respectively. The β values for the CF_3^+ (β = −1.0) and CH^+ (β = −0.91) strongly indicate that these energetic fragment ions are ejected in the direction perpendicular to the linear electric vector of the SR beam. That is, the approximate $\Delta\Lambda = \pm 1$ character in Eq. (1) is still valid for the $\pi^* \leftarrow$ C1s(CCH) excitation of the polyatomic CF_3CCH. The β values of CF_2^+ and CF^+ approach zero because they are produced through two and three bonds dissociation in releasing heavy F atom(s), respectively.

The central parts with KE ≅ 0 in the C_2H^+ and CF_3^+ profiles are weak at $h\nu$ = 295.4 eV. The C_2H^+ peak has the wings in the parallel direction (Fig. 2b). The β values deduced for the energetic CH^+, C_2H^+, CF_2^+, and CF_3^+ ions were β = 0.45, 0.37, 0.34, and 0.31, respectively, all being positive. We assigned thus the photoabsorption peak at 295.4 eV to the $\sigma^*_{CF} \leftarrow$ C1s(CF) transition which has the approximate $\Delta\Lambda = 0$ character. In the same way the photoabsorption peak at 294.0 eV is assigned to the $\pi^* \leftarrow$ C1s(CF) transition (see Table 1) since the β values of the fragment ions are negative. The peaks deconvoluted above 296 eV are heavily overlapped and then evaluation of the β values is not easy. The anisotropy parameters for the fragment ions were close to zero. That is, the fragment ions are ejected in an isotropic direction in this energy region.

3.3. Kinetic energy distributions

Kinetic energy distributions of the fragment ions were derived from the peak fitting analyses. The upper panels in Fig. 3 indicated by solid circles show the kinetic energy distributions of the H^+, CH^+,

C_2H^+, CF_2^+, and CF_3^+ fragment ions formed at the $\sigma^*_{CF} \leftarrow$ C1s(CF) transition and the lower ones indicated by solid squares are those at the $\pi^* \leftarrow$ C1s(CCH) excitation. The kinetic energy distributions of the H^+, CH^+, C_2H^+, and CF_2^+ fragment ions are approximated by using a Gaussian function and found to have the maxima at KE = 5.3, 3.6, 2.5, and 1.2 eV, respectively, in both the σ^*_{CF} and π^* excitations. The peak maxima are understood by simple mass ratios: $M(CH^+)/M(CF_2^+) \cong 1.2/3.6$ and $M(C_2H^+)/M(CF_2^+) \cong 1.2/2.5$, suggesting that the C–C bond dissociates in a short time and the axial recoil approximation is valid for the production of these energetic fragment ions.

The kinetic energy distribution of CF_3^+ formed in the $\sigma^*_{CF} \leftarrow$ C1s(CF) transition at 295.4 eV has two maxima at KE = 0.6 eV and 1.3 eV, which correspond to the $CF_3^+ + CH^+$ (or CH) and $CF_3^+ + C_2H^+$ (or C_2H)] dissociation channels since the mass ratios of $M(CH^+)/M(CF_3^+) \cong 0.2$ and $M(C_2H^+)/M(CF_3^+) \cong 0.4$ are close to the ratios of KE maxima observed: $0.6/3.6 \cong 0.2$ and $1.3/2.5 \cong 0.5$, respectively. The axial recoil approximation again holds in the C1s(CF) excitation of CF_3CCH. The probability of the former dissociation is 35% and that of the latter is 65% from the relative areas.

The kinetic energy distribution profile of CF_3^+ in the $\pi^* \leftarrow$ C1s(CCH) transition at 285.1 eV is largely different from that in the $\sigma^*_{CF} \leftarrow$ C1s(CF) excitation. Two peaks with the maxima at KE = 0.7 and 1.3 eV should correspond to the $CF_3^+ + CH^+$ (or CH) and $CF_3^+ + C_2H^+$ (or C_2H) pathways discussed just above, and the probabilities are 12 and 55%, respectively. The third component peaked at KE = 0 appears with the probability of 33%. The component peaked at KE = 0 may originate in the dissociation producing H^+ ion or H atom just as $CF_3^+ + H^+$ (or H) because the light atom takes away the greater part of excess energy and hence the heavy CF_3^+ ion with KE ≅ 0 would be left behind at the

C1s(CCH) site excitation. However, we believe that the contribution producing H^+ or H is small since the kinetic energy distributions of H^+ are similar in changing the excitation site from the C 1s of CF_3 to that of CCH (see Fig. 3). In addition, the relative yields of H^+, which will be discussed in the next section, are same at both the CF_3 and CCH excitation sites (see Table 2). The large change of the kinetic energy distribution of CF_3^+ formed by the C1s(CCH) excitation can be explained with the considerations argued in the core-excited CF_3CN [20]. That is, when the C1s(CF) electron is excited, the CF_3^+ fragment ions are spontaneously produced with KE ≅0.6 and 1.3 eV depending on the counterpart CH^+ (or CH) and C_2H^+ (or C_2H), respectively. At the C1s(CCH) excitation the CF_3^+ fragment ion is formed and at the same time a part of excess energy is distributed via the C–C≡C skeleton into the vibrational modes of CF_3. The CF_3^+ ions generated after the energy redistribution should have small kinetic energy and thus the anisotropy parameter in the ejection of CF_3^+ would approach zero as discussed in the previous section. That is, the CF_3 group in CF_3CCH probably works as an effective energy reservoir. Of course excess energy would flow from the initially excited C1s(CF) to the terminal CH group. However, the CH group has only one vibrational mode and then it is not an effective energy reservoir. The CH^+ and C_2H^+ fragment ions do not have a low KE ≅0 component as shown in Fig. 3.

3.4. Site-specific photofragmentation

Reflectron type TOF mass spectra are shown in Fig. 4 for two transitions at different sites: The σ^*_{CF} ← C1s(CF) at 295.4 eV and the π^* ← C1s(CCH) at 285.1 eV where the peak intensities were

normalized with the strongest CF^+. The mass spectrometer was fixed at the magic angle. The R-TOF mass spectra of the C1s(CF) edge observed at 293.8 (π*, not shown), 295.4 (σ^*_{CF}) and 297.0 eV (σ^*_{CF}, not shown) were little different and thus the state-dependent fragmentation is small. Table 2 shows the relative yields of the fragment ions. The main products are the C^+, C_2^+, CF^+, and CF_3^+ ions. The yields of the strongest CF^+ fragment ion are almost equal at the two sites. However, the yield of CF_3^+ at the C1s(CCH) excitation is 2 times as much as that at the C1s(CF) site, and the CF_2^+ fragment ion also shows a similar tendency. By contrast the yield of F^+ at the C1s(CF) site is 1.5 times as much as that at the C1s(CCH) excitation. The doubly charged C_3FH^{2+} and $C_3F_2H^{2+}$ ions at m/e = 28 and 37.5, respectively, are more produced at the C1s(CF) excitation. In general large fragment ions including $C_mF_n^+$ at $m/e \geq 44$ are easily formed by exciting the C1s(CCH) site. It is noticeable that the yields of C_3FH^+ (or $CFCCH^+$) and $C_3F_2H^+$ (or CF_2CCH^+) increases up to 2.7 and 4.2 times, respectively, by moving the exciting site from the C1s(CF) to C1s(CCH) though the yields are minor. These fragment ions should be formed via the C–F bond dissociation. That is, the CF_3 group works as an effective reservoir of intramolecular energy supplied from the initially excited C1s(CCH) atom, and then releases the F atom probably forming F_2, F or F^+. The observations are consistent with the kinetic energy distribution discussed in the previous section.

4. Concluding remarks

The total photoabsorption cross section of CF_3CCH was measured in the carbon K-shell region. The peak assignments were presented with the help of anisotropy parameters of fragment ions which were

deduced by a fitting method [28] applied to the angle-resolved L-TOF mass spectra. The kinetic energy distribution curves of the H^+, CH^+, C_2H^+, and CF_2^+ fragment ions were approximated by a Gaussian function with the maxima around 5.3, 3.6, 2.5, and 1.2 eV, respectively, both at the C1s(CCH) and C1s(CF) excitation sites. Kinetic energy distribution of the CF_3^+ formed at the C1s(CF) excitation has two maxima at KE ≅ 0.6 and 1.3 eV which correspond to the dissociation channels of $CF_3^+ + CH^+$ (or CH) and $CF_3^+ + C_2H^+$ (or C_2H) with the probabilities of 35 and 65%, respectively. However, the kinetic energy distribution of the CF_3^+ ion produced by exciting the C1s(CCH) electron changes to the profile showing three peak maxima at KE = 0, 0.7 and 1.3 eV, respectively, and their relative probabilities were 33, 12 and 55%. This observation was reasonably explained by the consideration that the formation of CF_3^+ competes with the intramolecular energy redistribution from the initially excited C1s(CCH) site to the terminal CF_3 group having vibrational modes that acts as an effective energy reservoir.

Site-specific fragmentation was observed in the R-TOF mass spectrometer mode. The doubly charged C_3FH^{2+} and $C_3F_2H^{2+}$ fragment ions were more produced at the C1s(CF) site excitation. The fragment ions larger than m/e ≥44 were more formed by exciting the C1s(CCH) site. Site-specific formation of $CFCCH^+$ and CF_2CCH^+ was consistent with the explanation that the CF_3 group acts as an energy reservoir.

Acknowledgements

The authors thank the staff of UVSOR at the IMS for the operation of the electron storage ring. This

work was supported by the IMS Joint Studies Program, a Grant-in-Aid on Research for the Future ‘Photoscience’ from Japan Society for the Promotion of Science and a Grant-in-Aid for Scientific Research from the Ministry of Education, Science, Sports, Culture and Technology of Japan.

References

[1] N. Saito, I.H. Suzuki, Phys. Rev. Lett. 61 (1988) 2740.

[2] K. Lee, D.Y. Kim, C.I. Ma, D.A. Lapiano-Smith, D.M. Hanson, J. Chem. Phys. 93 (1990) 7936.

[3] N. Saito, I.H. Suzuki, Phys. Rev. A 43 (1991) 3662.

[4] A. Yagishita, E. Shigemasa, Rev. Sci. Instrum. 63 (1992) 1383.

[5] N. Kosugi, E. Shigemasa, A. Yagishita, Chem. Phys. Lett. 190 (1992) 481.

[6] N. Kosugi, J. Adachi, E. Shigemasa, A. Yagishita, J. Chem. Phys. 97 (1992) 8842.

[7] E. Shigemasa, T. Hayaishi, T. Sasaki, A. Yagishita, Phys. Rev. A 47 (1993) 1824.

[8] A. Yagishita, E. Shigemasa, N. Kosugi, Phys. Rev. Lett. 72 (1994) 3961.

[9] J.D. Bozek, N. Saito, I.H. Suzuki, Phys. Rev. A 51 (1995) 4563.

[10] R.N. Zare, Mol. Photochem. 4 (1972) 1.

[11] R.L. Dehmer, D. Dill, Phys. Rev. A 18 (1978) 164.

[12] D. Dill, J.R. Swanson, S. Wallence, J.L. Dehmer, Phys. Rev. Lett. 45 (1980) 1393.

[13] J.D. Bozek, N. Saito, I.H. Suzuki, J. Chem. Phys. 98 (1993) 4652.

[14] J. Adachi, N. Kosugi, E. Shigemasa, A. Yagishita, J. Chem. Phys. 102 (1995) 7369.

[15] J. Adachi, N. Kosugi, E. Shigemasa, A. Yagishita, J. Chem. Phys. 107 (1997) 4919.

[16] N. Saito, K. Ueda, M. Simon, K. Okada, Y. Shimizu, H. Chiba, Y. Senba, H. Okumura, H. Ohashi, Y. Tamenori, S. Nagaoka, A. Hiraya, H. Yoshida, E. Ishiguro, T. Ibuki, I.H. Suzuki, I. Koyano, Phy. Rev. A 62 (2000) 042503.

[17] K. Okada, K. Ueda, T. Tokushima, Y. Senba, H. Yoshida, Y. Shimizu, M. Simon, H. Chiba, H.

Okumura, Y. Tamenori, H. Ohashi, N. Saito, S. Nagaoka, I.H. Suzuki, E. Ishiguro, I. Koyano, T. Ibuki, A. Hiraya, Chem. Phys. Lett. 326 (2000) 314.

[18] K. Okada, H. Yoshida, Y. Senba, K. Kamimori, Y. Tamenori, H. Ohashi, K. Ueda, T. Ibuki, Phys. Rev. A 66 (2002) 032503.

[19] T. Ibuki, K. Okada, T. Gejo, K. Saito, Chem. Phys. Lett. 328 (2000) 147.

[20] T. Ibuki, K. Okada, S. Tanimoto, K. Saito, T. Gejo, J. Electron Spectrosc. Relat. Phenom. 123 (2002) 323.

[21] A. Hiraya, E. Nakamura, M. Hasumoto, T. Kinoshita, K. Sakai, E. Ishiguro, M. Watanabe, Rev. Sci. Instrum. 66 (1995) 2104.

[22] R.N.S. Sodhi, C.E. Brion, J. Electron Spectrosc. Relat. Phenom. 34 (1984) 363.

[23] W.C. Wiley, I.H. McLaren, Rev. Sci. Instrum. 26 (1955) 1150.

[24] T. Ibuki, K. Okada, T. Gejo, K. Saito, J. Electron Spectrosc. Relat. Phenom. 101-103 (1999) 149.

[25] J.A.R. Samson, Techniques of Vacuum Ultraviolet Spectroscopy, Wiley, New York, 1967.

[26] W.L. Jolly, K.D. Bomben, C.J. Eyermann, At. Data Nucl. Data Tables 31 (1984) 433.

[27] A.P. Hitchcock, M. Tronc, A. Modelli, J. Phys. Chem. 93 (1989) 3068.

[28] N. Saito, I.H. Suzuki, Int. J. Mass Spectrum Ion Processes 82 (1988) 61.

[29] T. Gejo, E. Nakamura, E. Shigemasa, UVSOR Activity Report 1999 (2000) 39.

Table 1

Peak positions, term values, and proposed assignments for the total photoabsorption spectrum of CF_3CCH in the C K-shell region

Energy (eV)	Term Value (Quantum defect)					Assignment		
	C_H		C_{CC}		C_F	C_H	C_{CC}	C_F
285.1	6.9		7.4			π^*_{CC}	π^*_{CC}	
287.7	4.3	(1.2)	4.8			3s		
288.3	3.7		4.2	(1.2)			3s	
288.9	3.1		3.6			σ^*_{CH}		
289.2	2.8	(0.8)	3.3			3p	σ^*_{CC}	
290.1	1.9	(1.3)	2.4	(0.6)		4s	3p	
290.9	1.1	(0.3)	1.6	(1.1)		4p	4s	
291.6	0.4		0.9			Rydberg		
(292.0)						IP [a]		
292.4	-0.4		0.1				Rydberg	
(292.5)							IP [a]	
293.3	-1.3		-0.8		6.4		σ^*_{CC}	
294.0	-2		-1.5		5.7			σ^*_{CC}
294.7	-2.7		-2.2		5.0 (1.4)			3s
295.4	-3.4		-2.9		4.3			σ^*_{CF}
296.2	-4.2		-3.7		3.5 (1.0)			3p
297.0	-5		-4.5		2.7			σ^*_{CF}
297.7	-5.7		-5.2		2.0		σ^*_{CC}	
298.5	-6.5		-6		1.2 (0.6)	de [c]		$4p/\sigma^*_{CC}$
(299.7)								IP [b]
300.2	-8.2		-7.7		-0.5		de [c]	

[a] See the text for IPs.

[b] Taken from [26].

[c] Double excitation.

Table 2

Fragment ion yields (%) for site-specific excitation of the CF_3CCH molecule

Mass number (m/e)	Fragment ion	$\pi^* \leftarrow$ C1s(CCH) 285.1 eV	$\sigma^*_{CF} \leftarrow$ C1s(CF) 295.4 eV
1	H^+	2.6	2.6
12	C^+	8.7	11.7
13	CH^+	1.5	1.9
19	F^+	3.0	4.5
24	C_2^+	9.2	11.6
25	C_2H^+	6.2	7.3
28	C_3FH^{2+}	2.2	4.8
31	CF^+	23.4	21.6
36	C_3^+	3.2	3.7
37	$C_3H^+/C_3F_2^{2+}$	1.4	1.3
37.5	$C_3F_2H^{2+}$	5.2	7.7
43	C_2F^+	1.7	1.6
44	C_2FH^+	2.3	1.6
50	CF_2^+	5.6	4.7
55	C_3F^+	4.2	3.6
56	C_3FH^+	1.9	0.7
69	CF_3^+	12.1	6.2
74	$C_3F_2^+$	3.1	2.3
75	$C_3F_2H^+$	2.5	0.6

Figure captions

Fig.1. Total photoabsorption cross section of CF_3CCH in the carbon K-shell region and the anisotropy parameters (β) for fragment ions with high kinetic energies deduced by a fitting method [28] applied to the mass spectra recorded in linear TOF (L-TOF) mode shown in Fig. 2. The open circles in the top panel are the experimental data and the thin solid curves were obtained by a least squares curve fitting and the thick solid curve is the sum of them. The “de” means double excitation. The peak assignments in Table 1 and the estimated ionization potentials are shown.

Fig. 2. Experimental and calculated angle-resolved L-TOF mass spectra following excitation of the C1s(CF) and C1s(CCH) electrons into the vacant σ^*_{CF} and π^* levels at 295.4 and 285.1 eV, respectively. The open circles are the experimental data. The thin solid curves are the calculated profiles for different kinetic energies. The thick curve is the sum of the thin curves.

Fig. 3. Kinetic energy distributions of the H^+, CH^+, C_2H^+, CF_2^+, and CF_3^+ fragment ions in the $\sigma^*_{CF} \leftarrow$ C1s(CF) and $\pi^* \leftarrow$C1s(CCH) transitions shown by the solid circles and squares, respectively. The thin curves in CF_3^+ were obtained by a least-squares fitting. The thick curve is the sum of the thin curves.

Fig. 4. Reflectron type mass spectra at the $\sigma^*_{CF} \leftarrow$ C1s(CF) and $\pi^* \leftarrow$ C1s(CCH) transitions.

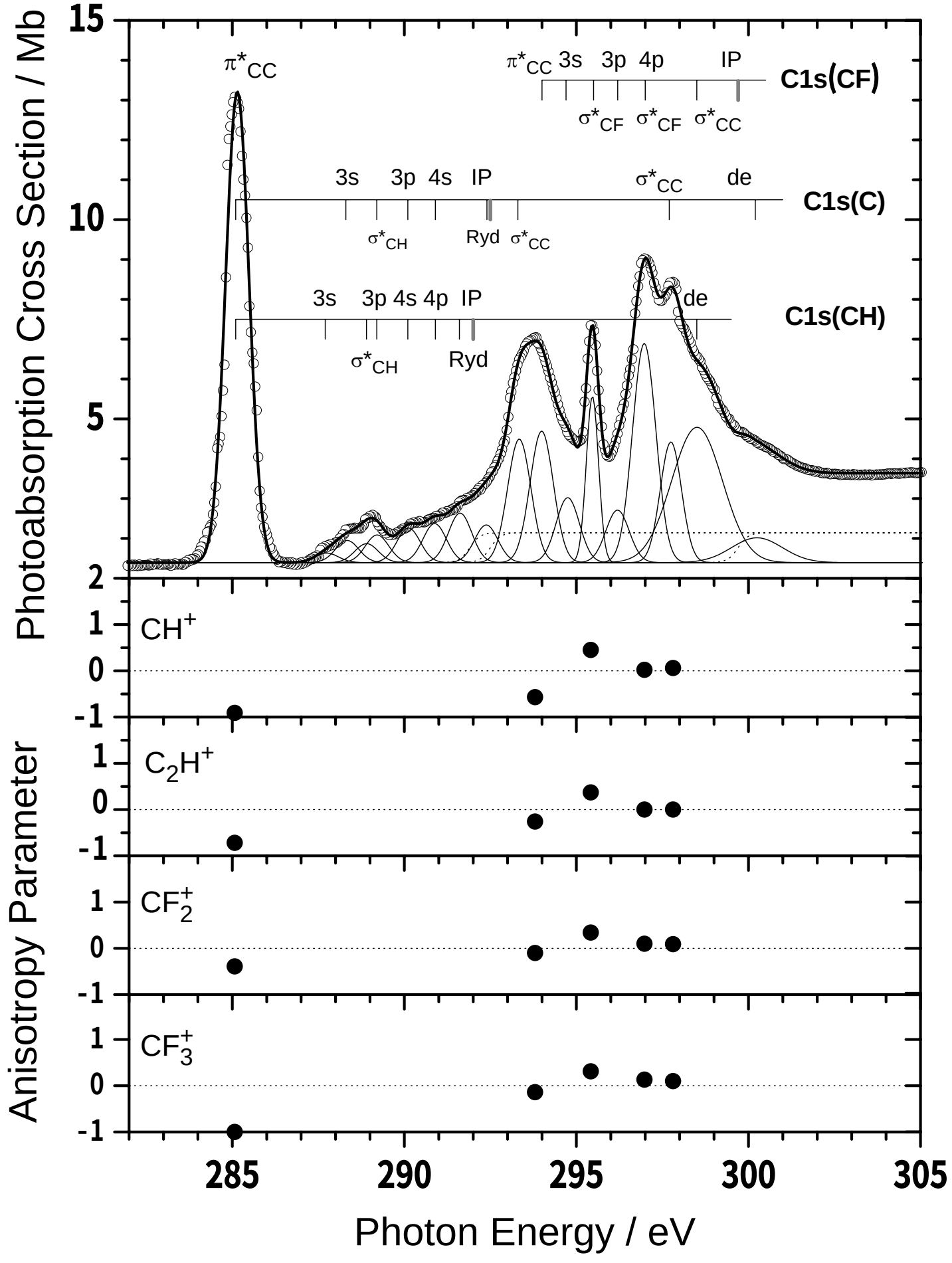
Photoabsorption Cross Section / Mb
Anisotropy Parameter
Photon Energy / eV
π*CC
π*CC 3s 3p 4p IP
C1s(CF)
σ*CF σ*CF σ*CC
3s 3p 4s IP
σ*CC de
C1s(C)
σ*CH Ryd σ*CC
3s 3p 4s 4p IP
de
C1s(CH)
σ*CH Ryd
CH+
C2H+
CF2+
CF3+
15
10
5
2
1
0
-1
285
290
295
300
305

Fig. 1.

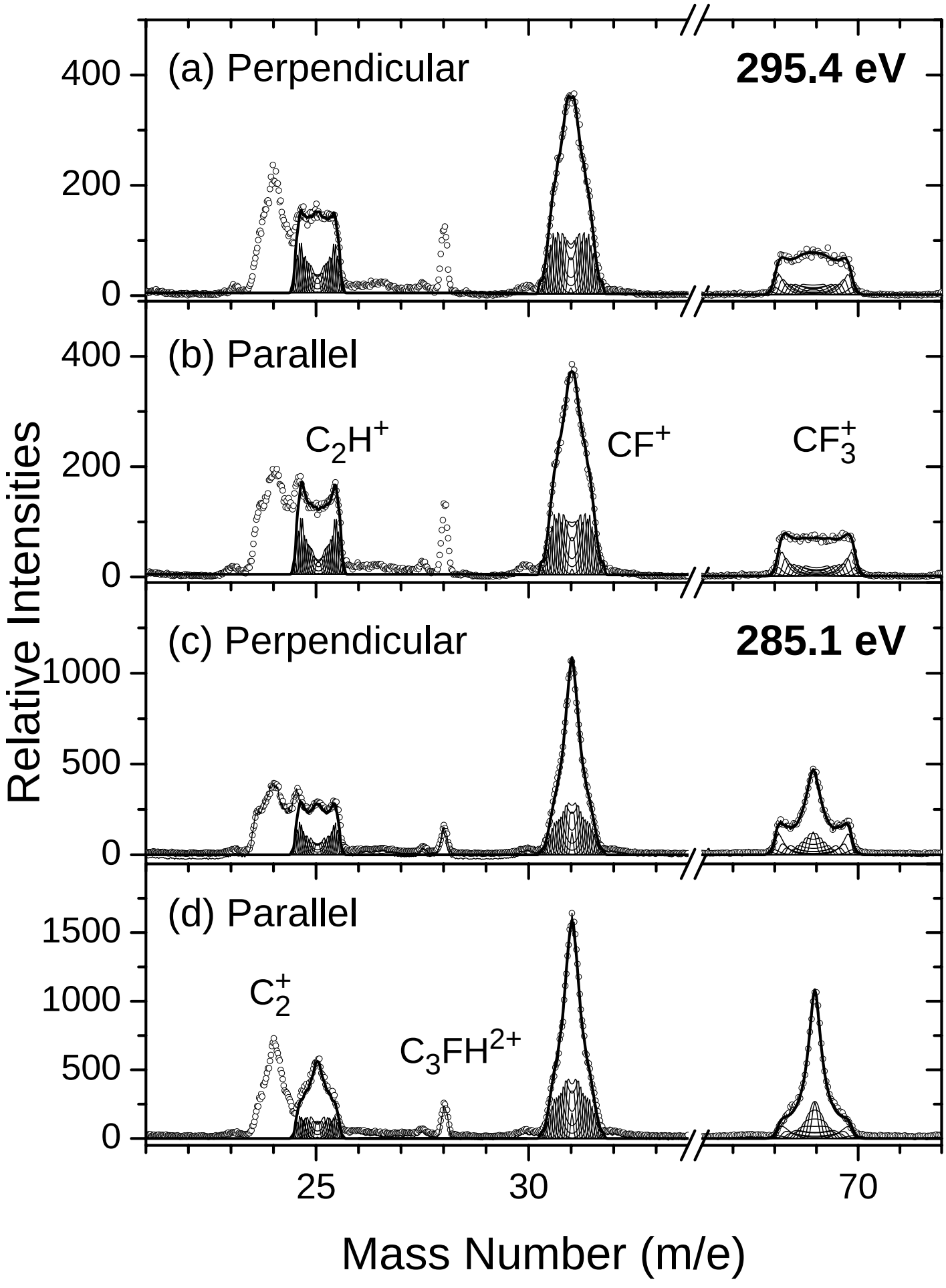
(a) Perpendicular
295.4 eV
(b) Parallel
C_2H^+
CF^+
CF_3^+
(c) Perpendicular
285.1 eV
(d) Parallel
C_2^+
C_3FH^{2+}
Relative Intensities
Mass Number (m/e)
400
200
0
1000
500
1500
25
30
70

Fig. 2.

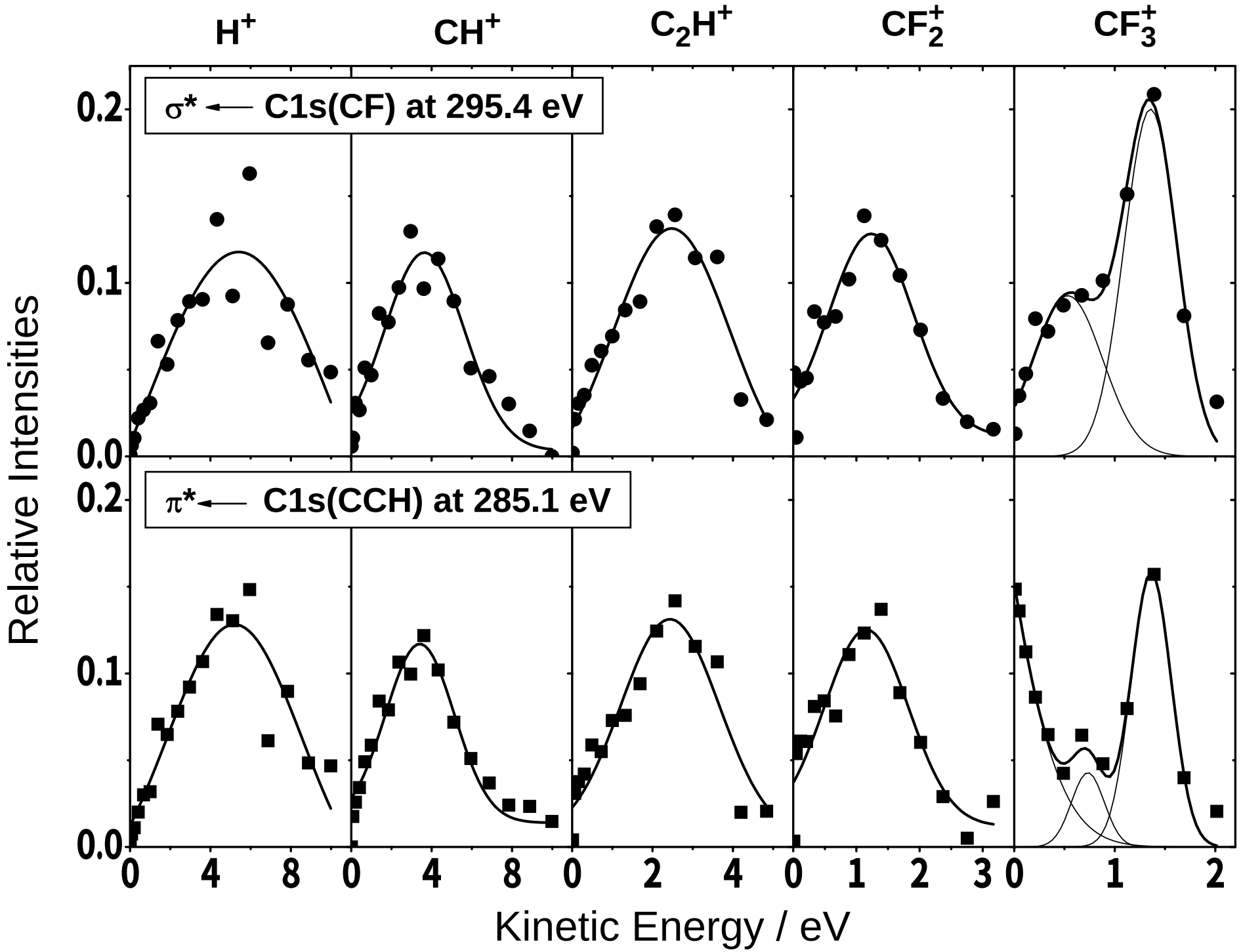
H+
CH+
C2H+
CF2+
CF3+
σ* ← C1s(CF) at 295.4 eV
π* ← C1s(CCH) at 285.1 eV
Relative Intensities
0.0
0.1
0.2
0
4
8
2
1
3
Kinetic Energy / eV

Fig. 3

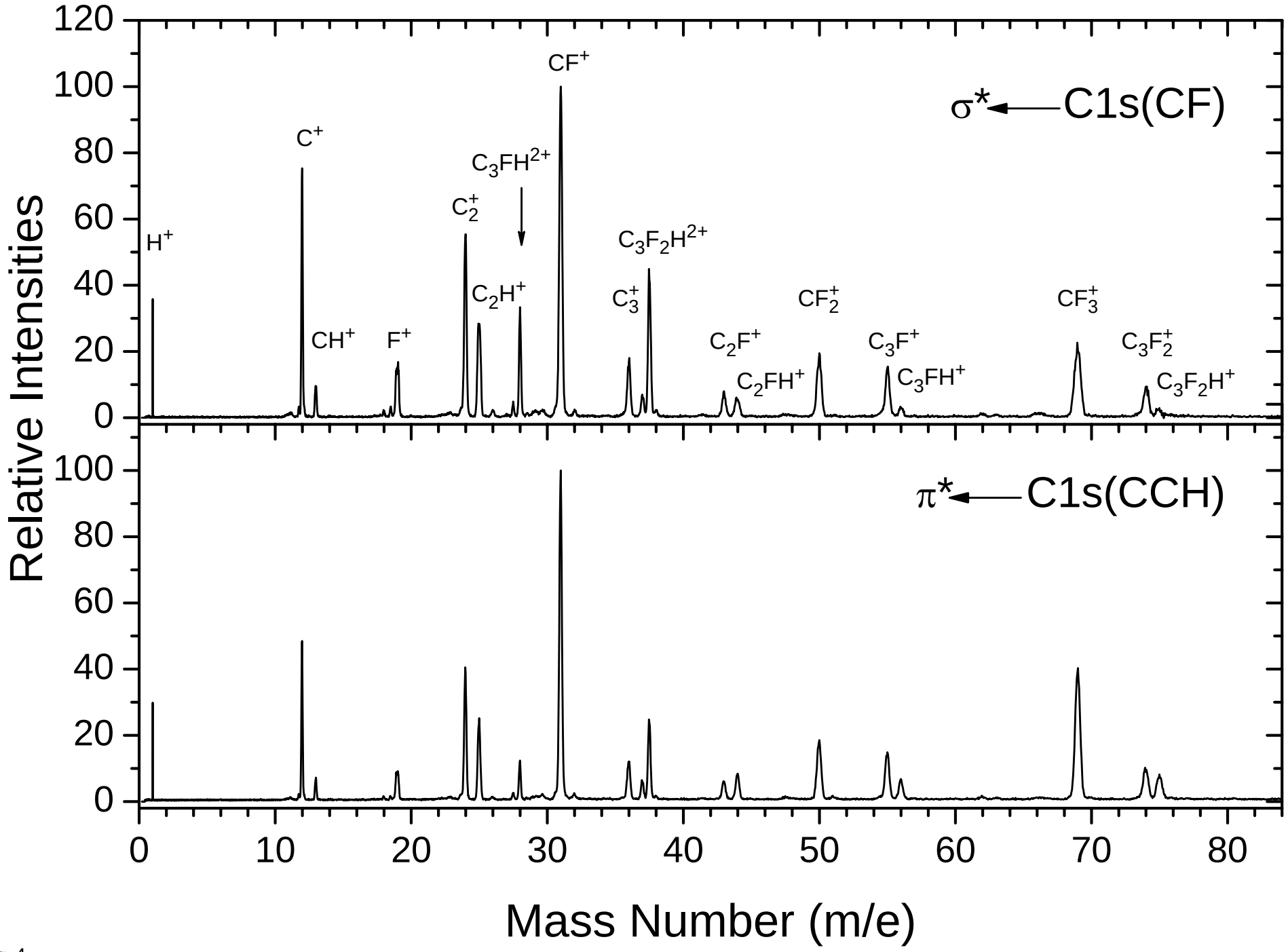
Relative Intensities
Mass Number (m/e)
σ*←C1s(CF)
π*←C1s(CCH)
H+
C+
CH+
F+
C2+
C3FH2+
C2H+
CF+
C3F2H2+
C3+
C2F+
C2FH+
CF2+
C3F+
C3FH+
CF3+
C3F2+
C3F2H+

Fig. 4